

Lagrangian simulations of pollutants under conditions of bora and sirocco winds in the middle Adriatic using FLEXPART-WRF models

Denk, Luka

Master's thesis / Diplomski rad

2022

Degree Grantor / Ustanova koja je dodijelila akademski / stručni stupanj: **University of Split, University of Split, Faculty of science / Sveučilište u Splitu, Prirodoslovno-matematički fakultet**

Permanent link / Trajna poveznica: <https://urn.nsk.hr/urn:nbn:hr:166:487672>

Rights / Prava: [Attribution-NoDerivatives 4.0 International/Imenovanje-Bez prerada 4.0 međunarodna](#)

Download date / Datum preuzimanja: **2024-07-18**

Repository / Repozitorij:

[Repository of Faculty of Science](#)



UNIVERSITY OF SPLIT
FACULTY OF SCIENCE

MASTER'S THESIS

**Lagrangian simulations of pollutants under
conditions of bora and sirocco winds in the
middle Adriatic using FLEXPART-WRF models**

Luka Denk

Split, February 2022

ACKNOWLEDGEMENT

I would like to thank my thesis advisor Prof. Dr. Sc. Darko Koraćin for his patience and help during the writing of this thesis. He allowed me to work at my own pace and helped me obtain the data for the simulations.

Special thanks to Dr. Alexandros-Panagiotis Poulidis of the University of Bremen who helped me access the resources of the University of Bremen and taught me the basics of FLEXPART.

Many thanks to ERASMUS + programme for giving me the opportunity and the support to study abroad.

Dr. John Mejia is acknowledged for providing the WRF simulation results.

Finally, I must express gratitude to my girlfriend Mia who supported me during my studies, and my father Branimir for his tolerance and continued help. I could not have done it without them.

Temeljna dokumentacijska kartica

Sveučilište u Splitu
Prirodoslovno – matematički fakultet
Odjel za fiziku
Ruđera Boškovića 33, 21000 Split, Hrvatska

Diplomski rad

Lagranžijanske simulacije onečišćenja pod uvjetima bure i juga nad srednjim Jadranom pomoću FLEXPART-WRF modela

Luka Denk

Sveučilišni diplomski studij Fizika, smjer Fizika okoliša

Sažetak:

Urbana aglomeracija oko Kaštelanskog zaljeva je po naseljenosti druga najveća u Hrvatskoj. U ovom radu su proučene karakteristike disperzije polutanata nad istočnim Jadranom. FLEXible PARTicle disperzijski model (FLEXPART) je korišten za simulaciju kretanja čestica tokom bure i juga. Ulazni parametri su meteorološki podaci dobiveni iz simulacija Weather Research and Forecasting (WRF) modelom.

Tokom bure oblak se kreće u smjeru zapad-jug-zapad, iako ne konzistentno, jer bura puše na mahove. Najveće koncentracije su izmjerene na području Splita, blizu ispusta. Koncentracije veće od $2 \mu\text{g}$ se ne pojavljuju dalje od Šolte, udaljene 20-ak kilometara. Oblak se vertikalno miješa do 2 kilometra visine 12 sati nakon početka događaja.

U slučaju juga, oblak se kreće u smjeru sjever-sjever-zapad, najviše preko Kaštela i kreće se niže te miješa sporije nego za bure. Ukupna masa polutanata u domeni je manja u slučaju bure nego juga što daje naslutiti veću prosječnu brzinu juga od bure pošto je jednaka masa puštena u atmosferu u oba slučaja. Koncentracije više od $2 \mu\text{g}$ pojavljuju se u Kaštelima, Splitu, Šolti, Trogiru te čak 60 kilometara sjeverozapadno od točke ispusta.

- Ključne riječi:** Lagranžijanske simulacije, disperzija, FLEXPART, WRF, bura, jugo, Split, istočni Jadran
- Rad sadrži:** 41 stranica, 19 slika, 19 literaturnih navoda. Izvornik je na engleskom jeziku
- Mentor:** prof. dr. sc. Darko Koračin
- Ocjenjivači:** Prof. dr. sc. Darko Koračin
Doc. dr. sc. Petar Stipanović, član
Dr. sc. Slavko Radilović, Državni hidrometeorološki zavod RH, član, vanjski član
- Rad prihvaćen:** 14.02.2022.

Rad je pohranjen u knjižnici Prirodoslovno – matematičkog fakulteta, Sveučilišta u Splitu.

Basic documentation card

University of Split
Faculty of Science
Department of Physics
Ruđera Boškovića 33, 21000 Split, Croatia

Master's thesis

Lagrangian simulations of pollutants under conditions of bora and sirocco winds in the middle Adriatic using FLEXPART-WRF models

Luka Denk

Graduate university program Physics; specialisation: Environmental Physics

Abstract:

Urban agglomeration around Kaštela Bay is an area with the second-highest population in Croatia. In this master's thesis, characteristics of dispersion of pollutants across the Eastern Adriatic are examined. FLEXible PARTicle dispersion model (FLEXPART) is used to simulate the movement of particles during bora and sirocco wind episodes provided by the Weather Research and Forecasting (WRF) model.

During the bora event, plume moved towards the west-south-west, although not constantly with the same precision due to the bora being a gusty wind. Maximum concentrations were in the Split area, closest to the release points. Concentrations higher than $2 \mu\text{g}$ did not extend past Šolta island, some 20 kilometres away. The plume was quickly dispersed vertically, up to 6 km, in the span of 12 hours after the start of the event.

The plume during the sirocco case moved towards the north-north-west, mostly over Kaštela, and it exhibited lower vertical dispersion up to 2 km compared to the bora event. Total mass in the domain was lower, indicating higher average wind velocity since the same mass was emitted in both cases. Concentrations higher than $2 \mu\text{g}$ are simulated in Kaštela, Split, Šolta, Trogir, and even 60 kilometres north-west of the release points.

Keywords: Lagrangian dispersion simulations, FLEXPART, WRF, bora, sirocco, Split, eastern Adriatic

Thesis consists of: 41 pages, 19 figures, 19 references. Original language: English

Supervisor: Prof. Dr. Darko Koračin

Reviewers: Prof. Dr. Darko Koračin
Assist. Prof. Dr. Petar Stipanović
Dr. Slavko Radilović

Thesis accepted: 14.02.2022

This thesis is deposited in the library of the Faculty of Science, University of Split.

Contents

1.	Introduction	1
2.	Characteristic winds over Eastern Adriatic	3
2.1.	Bora	3
2.2.	Sirocco	4
3.	Methodology.....	6
3.1.	Lagrangian modelling.....	6
3.2.	Dispersion modelling.....	7
3.3.	Lagrangian particle dispersion models (LPDM)	8
3.4.	FLEXPART	9
3.5.	Weather Research and Forecasting model (WRF)	10
3.6.	FLEXPART-WRF	11
3.6.1.	User input	12
3.6.2.	Parameterization	12
4.	Experiment setup	14
4.1.	Synoptic situation	17
5.	Discussion.....	19
5.1.	Dispersion simulations during bora wind episode.....	19
5.2.	Dispersion simulations during sirocco wind episode	25
6.	Conclusion.....	31
8.	Literature	32
9.	Appendix	34
9.1.	Bora input file:.....	34
9.2.	Sirocco input file	38

1. Introduction

The Adriatic Sea is the northernmost arm of the Mediterranean located between the Apennine Peninsula and the Balkans that extends from the Po Valley to the Strait of Otranto. The Western Italian coast is smooth while the Eastern, Croatian coast is characterized by complex topography, being the most indented coastline in the Mediterranean with over 1200 islands and many headlands rising abruptly from the deep water.

The two most important winds are bora and sirocco, both of which are transient phenomena, lasting several days. Both winds are often connected with migrating cyclones (Orlić et al., 1994.)

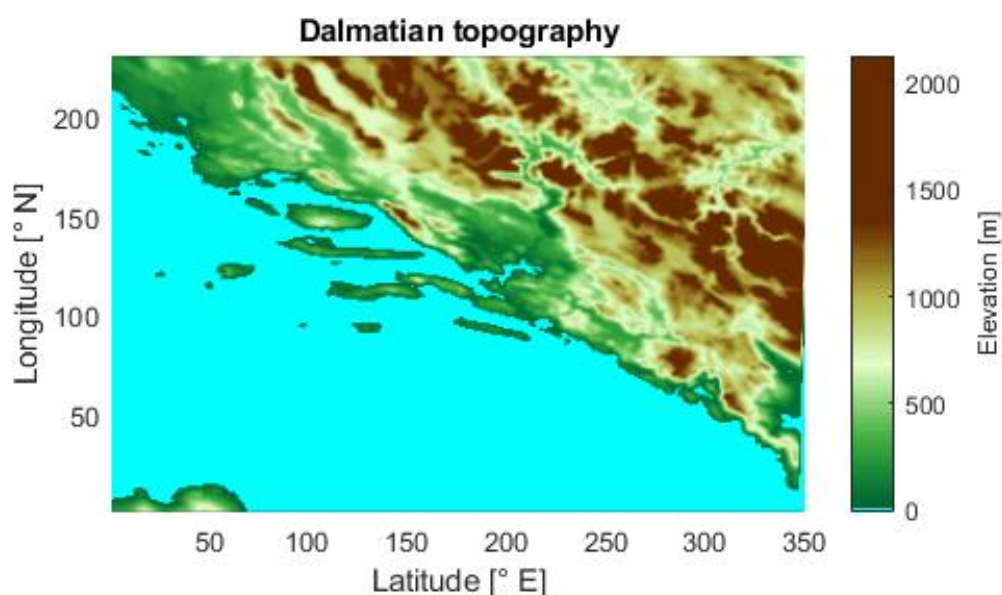


Figure 1. Topography of central Dalmatia

According to the Air quality assessment for the Republic of Croatia for 2017., major pollutants in the middle Adriatic are O_3 whose concentration are higher than the long-term prescribed limits, and PM_{10} whose concentration exceeds both lower and upper assessment thresholds several times a year. PM_{10} concentrations are higher than the prescribed thresholds for exceedances in Croatia (Zagreb, Split, Rijeka and Osijek). A lower assessment threshold refers to a level beyond which there is a risk to human health from brief exposure for particularly sensitive sections of the population while an upper assessment threshold

refers to a limit beyond which there is a risk to human health for general population from brief exposure.

This study investigates the interaction between atmospheric pollutants emitted in the eastern Adriatic (Split area) during bora and sirocco wind episodes. FLEXPART-WRF Lagrangian particle dispersion model, forced by wind fields obtained from the Weather Research and Forecasting (WRF) meteorological model, is used to determine the pollutant dispersion characteristics. The main characteristics and climatology of bora and sirocco winds will be given to provide an insight into the impact of winds on dispersion characteristics. A chapter is dedicated to describing Lagrangian modelling and the FLEXPART model as well as the WRF modelling system. This is followed by the description of the experiment: FLEXPART and WRF parameter setup and input data will be discussed. Results will be presented and discussed. Finally, the conclusion will summarize the most important findings of this thesis.

2. Characteristic winds over Eastern Adriatic

Adriatic winds are significantly influenced by the land-sea interaction as well as orography in the sense that they would change their nature, strength, and extent and they are always related to a certain synoptic situation governed by the pressure gradient (Ulbrich et al.: Climate of the Mediterranean, 2012.). The Adriatic winds are mainly downslope and gap flow winds or thermally induced circulation (Romanic, 2018.). Most important and well-known winds are bora, sirocco, mistral, tramontana, etesian. This thesis will consider the two strongest and most frequent winds: bora and sirocco.

2.1. Bora

Bora (Greek: *boréas* - north wind) is a type of severe downslope wind which blows mainly during the cold season across the eastern Adriatic. It is a synoptically and orographically generated wind flowing from the north-east over the coastal mountains down to the Adriatic. Bora has a substantial effect on human activities and in some cases safety is an issue as the mean speed during severe bora events can surpass 30 m/s with wind gusts which can reach twice the mean speed (the strongest measure bora gust was 69 m/s). It starts suddenly and blows over the coastal mountains that are ~1 km in height bringing air that is colder and drier than that on the lee side of the mountains (Ulbrich et al., 2012.). The air originates from the continent, usually from the broader Pannonian area and central Europe. Synoptic situations during bora events are well known; the bora can be forced by a cyclone south-west of the affected region (“dark bora”), an anticyclone north or north-east of the affected region (“clear/white bora”), or a cold front passage, which induces a relatively short event. Although the bora can occur during the whole year the highest frequency is during the cold season when it is also the most vigorous; it is not unusual for the events to last up to four to six days. Regarding the height at which it can occur the bora can be classified either as shallow or deep. A shallow bora occurs when the flow is trapped in the lower troposphere, e.g., by a strong synoptic inversion from the flow aloft. An example is a bora associated with a ridge from the Siberian anticyclone. Deep bora blows throughout the troposphere and is on average weaker than the shallow bora, although proper climatology is lacking (Grisogono and Belušić, 2009). Bora can also be generated by Alpine lee cyclo-

genesis, primarily around the Gulf of Genoa and the “daughter cyclone” in the Adriatic. Depending on the intensity of such lee-cyclogenesis, bora can be either deep or shallow.

Bora used to be understood as a katabatic-type flow, blowing down the mountains due to the effect of gravity (Orlić et al., 1992.). With ALPEX (“The Alpine Experiment”) started the change of this understanding (Grisogono and Belušić, 2009).. Now it is described as a hydraulic-type flow (Ulbrich et al., 2012.). If simplified, it can be said that the bora blows over moderately high mountains that partially block the airflow causing steep waves to appear above the mountain, overturn and eventually break. Following this hydraulic jump-like structures form in the lower lee side (Belušić et al., 2013). Strong winds mentioned above occur in the lowest troposphere and are located below the primary wave-breaking region.

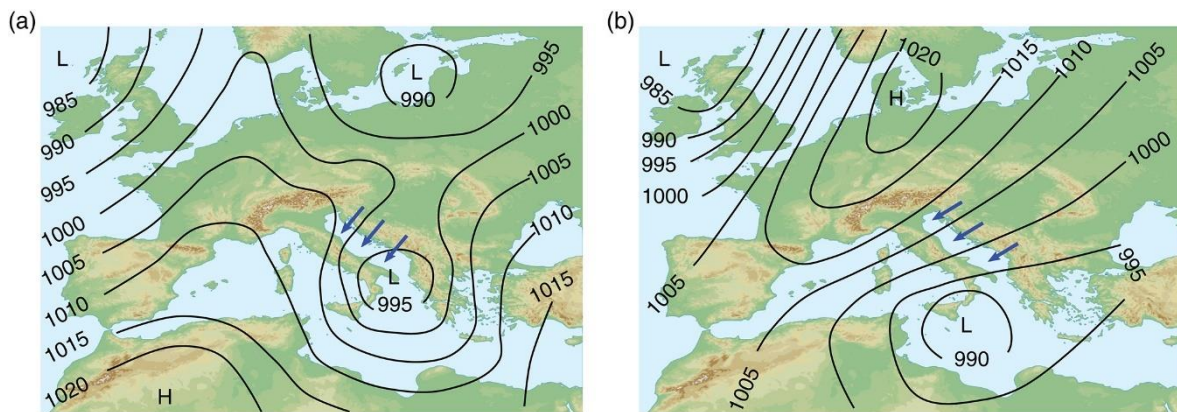


Figure 2. Schematic mean sea level pressure maps of typical synoptic situations during (a) cyclonic and (b) anticyclonic bora (Romanic, 2018)

2.2. Sirocco

Sirocco, locally called jugo (Croatian: *jug* - south) is a south-to-south-easterly warm and moist wind over the Adriatic which is confined by the Apennines to the west and the Dinaric Alps to the east. It can reach average gale speeds with highest speeds occurring on the open sea, but during the peaks of its events it can cause storm surges and it has been shown that the build-up of water can cause flooding, especially in Venice. In contrast to bora, jugo increases in strength gradually as it is caused by large-scale weather patterns. Gusts can occur due to sub-synoptic effects such as orography and instabilities at the interface between the land and sea regions. Jugo is also more frequent and stronger in the

colder part of the year and can last up to three days during the summer and longer than a week during winter. This weather phenomenon as it vertically extends up to 2 km.

Jugo is generated by larger-scale weather patterns and can be classified under two categories: anticyclonic and cyclonic. Cyclonic type is more frequent and is most often related to the Genoa cyclone, north-west of the affected area, and brings low, dark clouds with plenty of rain. Anticyclonic jugo is primarily forced by the pressure gradient between the low-pressure field north-west of the Adriatic and the high-pressure field above the eastern Mediterranean, and brings nicer weather than the cyclonic Jugo.

A short remark about the difference between sirocco and jugo should be said. Although jugo is usually considered to be a variation of the sirocco wind system, an argument was put forward by Jurčec *et al.* (1996) and Ivančan-Picek *et al.* (2006) that this is not the case. Sirocco as defined by the Glossary of Meteorology as a warm south or south-east wind in advance of a depression moving eastward across the southern Mediterranean Sea or North Africa. It has origins in Northern Africa and carries dust particles with it. Although sirocco can reach eastern Adriatic shores, jugo is not generally associated with the cyclone in the southern Mediterranean or North Africa and it is not usually weakening when reaching the Adriatic shores.

This study will use the terms sirocco and jugo interchangeably since it is not the point of it to determine if they are one and the same.

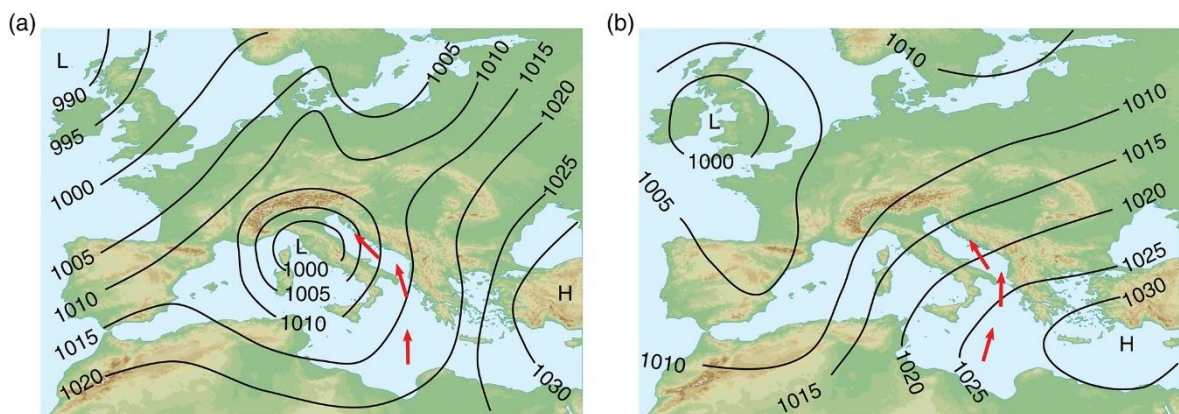


Figure 3. Schematic mean sea level pressure maps of typical synoptic situations during (a) cyclonic and (b) anticyclonic jugo (Romanic, 2018)

3. Methodology

3.1. Lagrangian modelling

There are Eulerian and Lagrangian approaches when modelling fluids. Eulerian models work on a fixed computational grid and cannot resolve anything smaller than its grid spacing, which makes tracking individual parcels impossible. The properties at a certain point are interpolated inside the grid. Lagrangian models on the other hand follow each parcel individually. The grid in this approach is not fixed and an observer “moves” with the flow. This allows for tracking of each parcel, but the parcels do not interact with each other unless Lagrangian chemistry is included.

Consider the case of some property q of flow in a small box of fluid (Figure 4). If q can change continuously in time and space the relationship between q_{in} and q_{out} in the X direction is

$$q_{out} = q_{in} + \frac{\partial q}{\partial t} \delta t + \frac{\partial q}{\partial x} \delta x$$

The rate of total change q within the box is

$$\frac{dq}{dt} = \frac{q_{out} - q_{in}}{\delta t} = \frac{\partial q}{\partial t} + \frac{\partial q}{\partial x} \frac{\delta x}{\delta t}$$

In three dimensions the operator becomes

$$\frac{d}{dt} = \frac{\partial}{\partial t} + \mathbf{u} \cdot \nabla$$

The operator consists of two contributing parts: local change $\partial q/\partial t$ and an advective part $\mathbf{u} \cdot \nabla$. This transformation from coordinates following a parcel to coordinates fixed in space converts a simple linear derivative into a non-linear partial derivative.

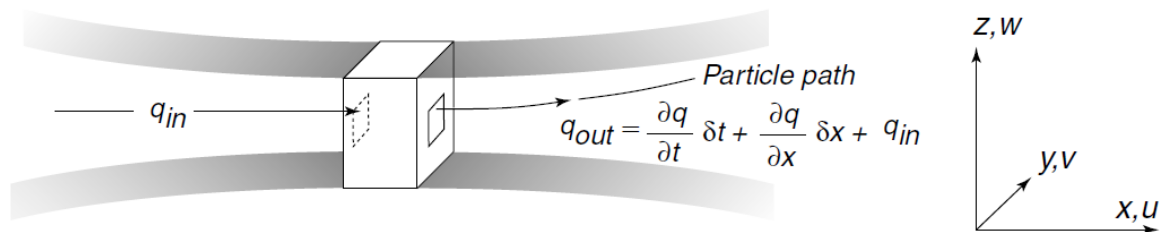


Figure 4. Sketch of the flow used for deriving the total derivative (Introduction To Physical Oceanography, R. H. Stewart. 2000.)

Eulerian models have fixed coordinate grids and calculate properties of the fluid (velocities, concentrations, pressure, etc.) at fixed nodes of the grid so the observer is said to be fixed. Lagrangian models calculate coordinate position of parcels at each time step and observer is said to move with them. The value of q at any point in the domain can be interpolated from the nearest parcels or by averaging within grid cells, depending on the number of parcels in the region. For this method to work, the domain must be uniformly covered by a sufficiently dense number of parcels for both approaches. This becomes a problem for the Lagrangian approach as the convergence and divergence of the flow may depopulate some regions of the domain even if an initial distribution is given. Algorithms are required to eliminate parcels where they are redundant and to add new ones where needed.

Roughly, the required number of parcels for a Eulerian model is $(DSL^{-2}H^{-1})$, where L and H are horizontal and vertical scales respectively with surface and depth given by S and D . However, Lagrangian models require 10-100 times more parcels since they tend to cluster together. This makes Lagrangian calculation of the flow computationally expensive (Cushman-Roisin and Beckers, 1994).

3.2. Dispersion modelling

Air quality is closely related to human health in the modern world, especially in heavily populated, urban areas. Predicting pollutant concentrations and determining its sources thus became an important knowledge to have. All dispersion models can be categorized as either source or receptor models. Source type (forward) models estimate downwind concentration given the emission rates and considering transport, dispersion, deposition, and chemical transformation processes. Receptor (backward) models estimate the source contributions given the measurements and calculating backwards in time. Both source and receptor models are complementary and compensate for each other's weaknesses. Two main different types of models are Eulerian and Lagrangian. Eulerian source models can represent complex chemistry and interaction among source emissions, but are limited in their representation of dispersion and numerical accuracy. Lagrangian models more accurately represent transport and dispersion on multiple scales, and they exhibit minimal numerical diffusion, but chemical processes and physical processes involving mixing are difficult to implement in their algorithms.

This thesis focuses on Lagrangian forward type modelling.

3.3. Lagrangian particle dispersion models (LPDM)

A Lagrangian model in a forward mode simulates the transport and diffusion of atmospheric pollutants by computing trajectories of many individual particles from any number of sources and determines concentrations at a prescribed receptor. The basic algorithm is given in Koraćin et al. (2011).

Hypothetical particles are released at a given rate and their new position is calculated after a time step Δt by using the standard random displacement method:

$$\begin{aligned}x(t + \Delta t) &= x(t) + [u(t) + u_r(t)]\Delta t \\y(t + \Delta t) &= y(t) + [v(t) + v_r(t)]\Delta t \\z(t + \Delta t) &= z(t) + [w(t) + w_r(t)]\Delta t\end{aligned}$$

Here x , y and z are the particle positions, u , v and w are predicted mean components of the velocity along the X -, Y -, and Z -axes respectively. u_r , v_r and w_r are their respective subgrid-scale turbulent velocity components which are iteratively determined assuming a Markov random process based on the Langevin equation where the first term is the deterministic forcing (the memory term) and the second is a random forcing term

$$dv_{ti} = a_i(x, v_t, t)dt + b_{ij}(x, v_t, t)dW_j$$

as

$$\begin{aligned}u_r(t) &= u_r(t - \Delta t)R_u(\Delta t) + u_s(t - \Delta t) \\v_r(t) &= v_r(t - \Delta t)R_v(\Delta t) + v_s(t - \Delta t) \\w_r(t) &= w_r(t - \Delta t)R_w(\Delta t) + w_s(t - \Delta t)\end{aligned}$$

R_i are the Lagrangian autocorrelation functions for each velocity component, and u_s , v_s and w_s are the random fluctuations of the velocity components. The autocorrelation functions are given by

$$\begin{aligned}R_u(\Delta t) &= e^{-\Delta t/T_{Lu}} \\R_v(\Delta t) &= e^{-\Delta t/T_{Lv}} \\R_w(\Delta t) &= e^{-\Delta t/T_{Lw}}\end{aligned}$$

T_{Li} are the Lagrangian time scales for their respective velocity components determined from the scaling arguments:

$$T_{Lu} = z_i / \sqrt{(\overline{u'u'})_m}$$

$$T_{Lv} = z_i / \sqrt{(\overline{v'v'})_m}$$

$$T_{Lw} = z_i / \sqrt{(\overline{w'w'})_m}$$

Here z_i is the depth of the mixed layer, $(\overline{u'u'})_m$, $(\overline{v'v'})_m$ and $(\overline{w'w'})_m$ are the maximum variances in the domain, z_i is determined from the elevated minimum of the turbulence kinetic energy (TKE). The bounds for the random components are determined from the statistical properties of turbulent transfer and the following autocorrelation function

$$\sigma_u = \sqrt{(\overline{u'u'}) \cdot \{1 - R_u^2(\Delta t)\}}$$

$$\sigma_v = \sqrt{(\overline{v'v'}) \cdot \{1 - R_v^2(\Delta t)\}}$$

$$\sigma_w = \sqrt{(\overline{w'w'}) \cdot \{1 - R_w^2(\Delta t)\}}$$

σ_i are the standard deviations around zero mean for the range of random components u_s , v_s , and w_s respectively and $\overline{u'u'}$, $\overline{v'v'}$, and $\overline{w'w'}$ are the variances of the velocity components.

3.4. FLEXPART

LPDMs describe the transport and diffusion of tracers in the atmosphere by computing trajectories of large number of hypothetical particles. These particles represent infinitesimally small air parcels instead of physical particles. FLEXPART is an LPDM that simulates the long-range and mesoscale transport, diffusion, dry and wet deposition, and radioactive decay of tracers (Stoll et al., 2005.). It was originally developed in Norway. FLEXPART can be used either in forward or backward mode, depending on if the user wants to simulate dispersion from the source, or determine the source using given measurements. FLEXPART is an open-source (software available at <https://www.flexpart.eu/>) LPDM whose popularity can partly be attributed to a large number of user definable parameters, such as modelling domain, sources, release rates and particle distributions. Multiple sources can be active at the same time with different types of releases. A source can be either of point, line, or area geometry. Multiple types of particle species can be defined, such as ozone,

black carbon, NO, NO₂, Cs¹³⁷ and many more. Additionally, FLEXPART features different parameterization options which a user chooses before running the model.

FLEXPART uses meteorological model-level data from ECMWF (European Centre for Medium-Range Weather Forecasts) or pressure level data from National Centers for Environmental Prediction's (NCEP) Global Forecast System (GFS). Since FLEXPART was mostly used with input from global meteorological models, the implemented planetary boundary layer (PBL) turbulence parameterizations are based on data obtained from small-scale field experiments and are thus valid on mesoscale and local scales. This has inspired the creation of FLEXPART versions driven by mesoscale meteorological models output such as the Mesoscale Meteorological (MM5) model, the Weather Research and Forecasting (WRF) model, and the COSMO weather prediction model. The model version used in this thesis (FLEXPART-WRF v3.1) has mainly been developed at the University of Colorado Cooperative Institute for Research in Environmental Sciences (CIRES), in cooperation with the Norwegian Institute for Air Research (NILU), the Technical University of Catalonia Institute of Energy Technologies (INTE) and the University of Alaska Arctic Region Supercomputing Center (ARSC). FLEXPART-WRF is a useful tool to represent scales smaller than those FLEXPART-ECMWF/GFS can represent (Brioude et al., 2013).

3.5. Weather Research and Forecasting model (WRF)

The Weather Research and Forecasting modelling system is used for various forecast and analysis applications, from the microscale to the synoptic and global scales. It includes numerous parameterization options for boundary layer processes, convection, microphysics, radiation, and land surface processes, and several numerical scheme options. Initial and boundary conditions from other meteorological analysis systems are needed as WRF is a limited-area model. It of course has inherent uncertainties and limitations which propagate into the atmospheric transport modelling (Brioude et al., 2013).

WRF is a non-hydrostatic mesoscale model that uses perturbation equations with respect to a dry hydrostatic base state. Pressure based terrain-following coordinates are used. The prognostic variables are mass-weighted which helps to conserve mass. In order to achieve an accurate WRF output and thus an accurate FLEXPART-WRF simulation results, a careful choice of initial and boundary conditions, the land surface model, boundary layer scheme, and convection scheme is important.

3.6. FLEXPART-WRF

Adaptation of the original FLEXPART model, FLEXPART-WRF can handle WRF input data and different projections. To start a FLEXPART-WRF model run, different meteorological fields from WRF are required, as listed in the Table 1 below.

Table 1 WRF variables required by FLEXPART-WRF

WRF variable	dimension	description
ZNW	1-D	sigma value of full levels
ZNU	1-D	sigma value of half levels
PB	3-D	base value of pressure
P	3-D	perturbation of pressure
PHB	3-D	base value of geopotential
PH	3-D	perturbation of geopotential
T	3-D	temperature
QVAPOR	3-D	specific humidity
TKE	3-D	turbulent kinetic energy
XLAT	2-D	latitude
XLONG	2-D	longitude
MAPFAC_M	2-D	map factor
PSFC	2-D	surface pressure
U10	2-D	10 m wind along x axis
V10	2-D	10 m wind along y axis
T_2	2-D	2 m temperature
Q_2	2-D	2 m dew point
SWDOWN	2-D	surface solar radiation (optional)
RAINNC	2-D	large scale precipitation (optional)
RAINCL	2-D	convective precipitation (optional)
HFC	2-D	surface sensible heat flux (optional)
UST	2-D	friction velocity (optional)
PHLB	2-D	PBL height (optional)
if WIND_OPTION ≤ 0 is used		
U	3-D	wind along x -axis
V	3-D	wind along y -axis

<i>W</i>	3-D	Cartesian vertical velocity
if WIND_OPTION \leq 1 is used		
AVGFLX_RUM	3-D	mass-weighted, time-averaged wind along <i>x</i> -axis
AVGFLX_RVM	3-D	mass-weighted, time-averaged wind along <i>y</i> -axis
AVGFLX_RWWM	3-D	mass-weighted, time-averaged sigma dot
MU	2-D	perturbation of mass column
MUB	2-D	base value of mass column
if WIND_OPTION = 2 is used		
<i>U</i>	3-D	wind along <i>x</i> -axis
<i>V</i>	3-D	wind along <i>y</i> -axis
WW	3-D	Sigma dot

3.6.1. User input

All the user input is condensed into a single file which contains pathnames (for FLEXPART input and output), a list of operations, age classes used in the experiment, output coordinates and vertical levels, coordinates of the receptors, particle species (includes molar weight and deposition parameters, both wet and dry), and coordinates of release boxes. Numerous switches are available for the user, which control the output, terrain effect parameterization, convection schemes, turbulence options, and more.

3.6.2. Parameterization

Since the WRF model output is on an Arakawa C-grid with terrain-following pressure-based sigma levels and FLEXPART-WRF uses the unstaggered grid with Cartesian terrain-following coordinates, wind components must be interpolated onto the grid cell centres. FLEXPART-WRF has a subroutine that interpolates and applies correction factors. The exact procedure is described in Brioude et al. (2013).

The user can choose to either read the boundary layer parameters (the friction velocity u_* and the sensible heat flux) from the WRF output or let FLEXPART-WRF calculate them. WRF has different schemes to calculate PBL and the user needs to be aware of them. There also exists an option to include an additional term based on a subgrid-scale variation of topography. FLEXPART-WRF includes four options for turbulent wind parameterization. The first one turns the turbulence off and FLEXPART works as a non-dispersive Lagrangian

trajectory model. The second one internally calculates PBL turbulent mixing using the Hanna turbulence scheme (Hanna, 1982). The third and the fourth option use turbulent kinetic energy provided by the WRF but violate the well-mixed criterion and are advised not to be used by Brioude et al. (2013).

FLEXPART does not use WRF cloud fraction data. It instead diagnoses clouds based on relative humidity and adjusts scavenging coefficients based on the presence of clouds and precipitation. Dry deposition is simulated using land use and roughness length data.

Three choices are available for the format of FLEXPART-WRF output. First option outputs individual trajectory information. Second option outputs the centre of mass and clustered particle positions with additional information. Third option distributes the information from each particle onto a regular grid using a uniform kernel. This can be useful for comparing FLEXPART results with other model results. User is also given a choice of choosing the projection of the gridded output: first option is to follow WRF grid and second option defines a regularly spaced longitudes and latitudes.

4. Experiment setup

The simulation is made using FLEXPART-WRF Version 3.3.1, which uses the output from the WRF V4.2 meteorological model. Two runs were made, one for each wind event. Bora event lasted from 22. to 25. 02. 2019., and the Jugo event lasted from 11. to 13. 11. 2019. Meteorological runs were started 24 hours earlier in order for the WRF model to spin-up, that is to reach an equilibrium state, which is characterized by conditions in which no significant shifts in temperature and other parameters occur. Both runs started and ended at midnight with an output interval of 1 hour for a total of 121 time intervals in both cases. The spatial domain in both cases is the same. The Lambert conformal projection is centred around 42.9986°N and 17.3282°E. A horizontal spatial step of 1 km is used giving a grid of dimension 309×264. The total dimension of the meteorological domain is 309×264×69 grid cells.

Emissions in the Flexpart-WRF were set to start with the beginning of the simulation and finish 24 hours before the end. For particle species, black carbon is used, which represents PM₁₀ pollutant particles. Total emitted mass during a three day period is assumed 10000 kg for each release point since the real data was not accessible. Three sources of emissions were specified: Brodosplit shipyard in Split, Cemex cement plant in Kaštela, and AD Plastik factory in Solin.

Information used for the experiment run is summarized in the Appendix of the input files. More relevant information is given in the following Table 2:

During the bora run an error occurred which stated “richardson not working -- bad h”. It was solved by uncommenting the following lines in readwind.f90

```
do j = 0, nymin1
do i = 0, nxmin1
  duma = ps(i,j,1,n)
  dumdz = 0.5*(zzh(i,j,kgbn+1,n) - zzh(i,j,kgbn,n))
  tv = tth(i,j,kgbn,n)*(1.+0.61*qvh(i,j,kgbn,n))
  ps(i,j,1,n) = pph(i,j,kgbn,n)*exp( dumdz*ga/(r_air*tv) )
end do
end do
```

and in readwind_nests.f90

```
do j = 0, nyn(1)-1
do i = 0, nxn(1)-1
  duma = psn(i,j,1,n,1)
  dumdz = 0.5*(zzhn(i,j,kgbn+1,n,1) - zzhn(i,j,kgbn,n,1))
  tv = tthn(i,j,kgbn,n,1)*(1.+0.61*qvhn(i,j,kgbn,n,1))
  psn(i,j,1,n,1) = pphn(i,j,kgbn,n,1)*exp( dumdz*ga/(r_air*tv) )
end do
end do
```

in the model source code. This error appears if the pressure increases with height. Since bora is a turbulent event and the z levels were narrowly spaced, this occurred during the initial run.

During both runs the default source code has a maximum number of x- and y- grid points smaller than those used for these experiments so it was changed to 1000 in the file parmod.f90.

4.1. Synoptic situation

Meteorological data for both cases was based on real weather events. Late February in 2019 bora had hurricane force gusts and caused significant property damage along the Dalmatian coast, as wind gusts of 48.9 m/s were reported in Split. Synoptic situation can be seen in Figure 1Figure 5. A high-pressure field formed over Norway and moved southward while a low-pressure system formed over the Balkans and moved south-westward towards the Libyan coast. This resulted in a strong NE-SW gradient along which bora formed.

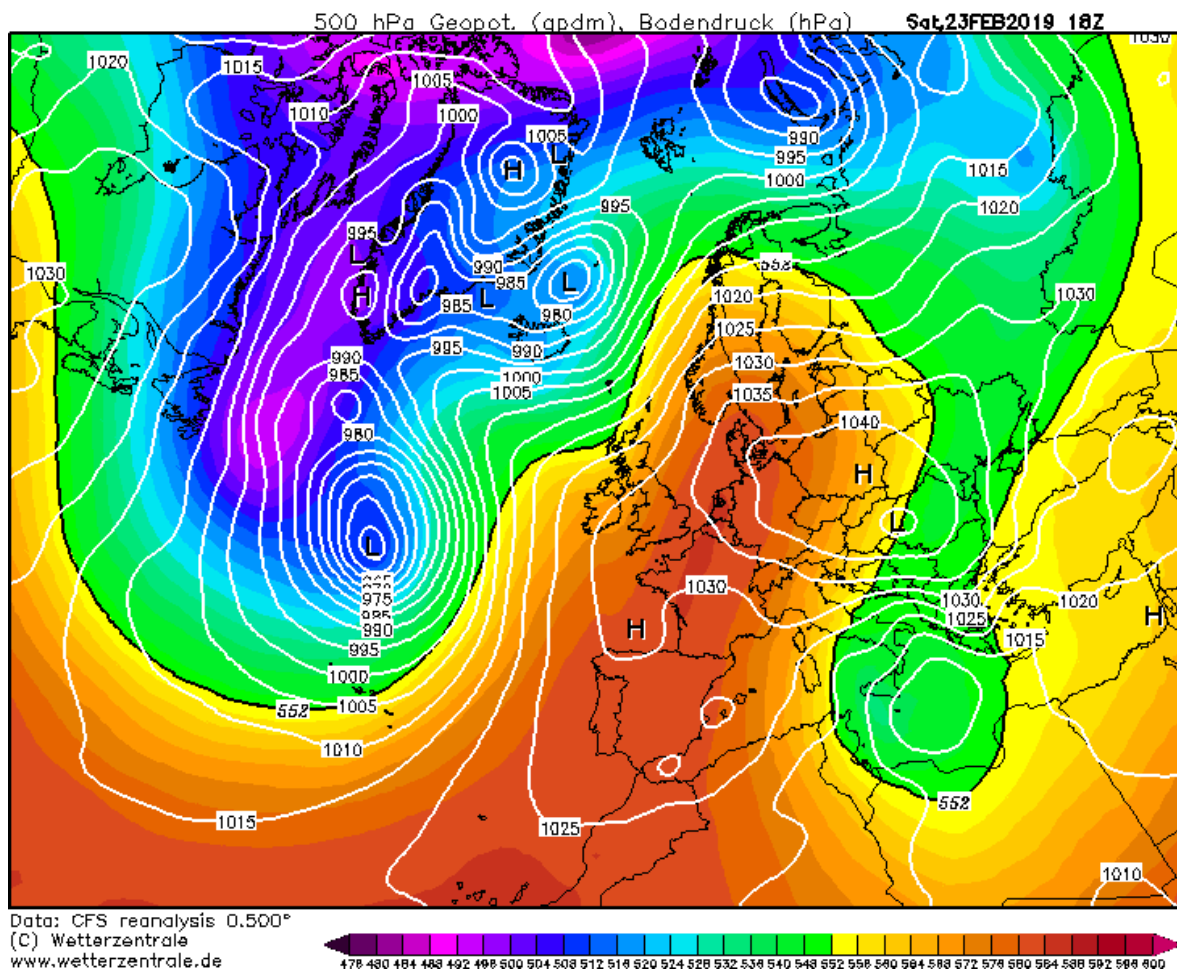


Figure 5. Synoptic situation over Europe and northern Atlantic during bora event, February 23, 2019. Strong surface pressure gradient between a high-pressure field over Poland and a low-pressure field south of Ionian Sea favoured the development of a strong bora.

(<https://www.wetterzentrale.de/reanalysis.php?map=1&model=cfsr&var=1&jaar=2019&maand=2&dag=23&h=0&nmaps=24>)

During November 10, 2019, a low-pressure system formed west of Sardinia and during the next day moved over Tunisia. It connected to a low-pressure system residing over Western Europe and created a deep trough that facilitated a gale cyclonic sirocco. This caused high sea levels all along the Dalmatian coasts, waves as high as 10 m in Dubrovnik, and a historic flood in Venice on November 13, 2019.

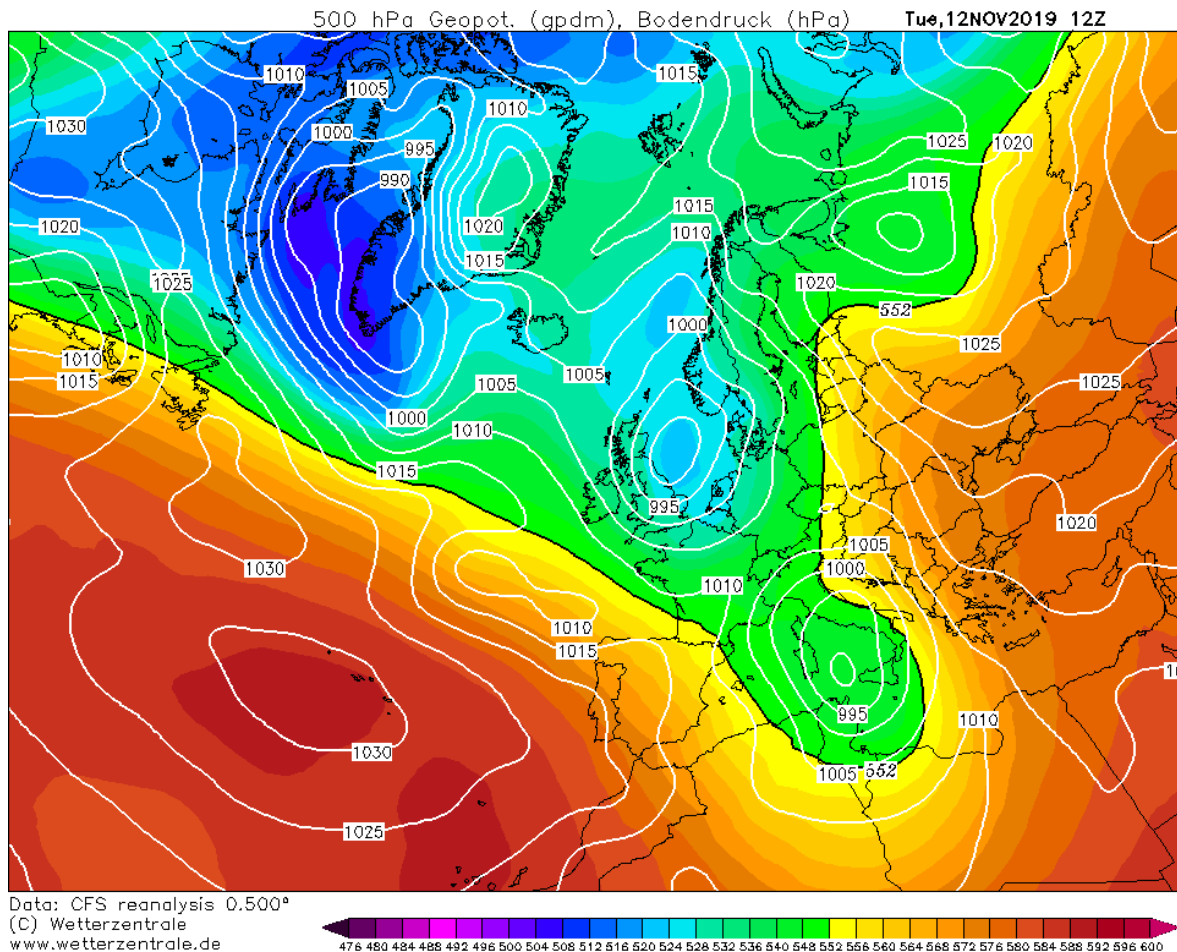


Figure 6. The synoptic situation over Europe and northern Atlantic during the sirocco event, November 11, 2019. Cyclonic sirocco was formed by a cyclone originating in Genoa Bay by a strong gradient along the Adriatic Sea which caused a severe sirocco event. The cyclone first travelled south and then retrograded back towards Italy, carrying warm African air and Mediterranean moisture causing a severe sirocco event that flooded Venice.

<https://www.wetterzentrale.de/reanalysis.php?jaar=2019&maand=11&dag=12&uur=1200&var=1&map=1&model=cfsr>

5. Discussion

5.1. Dispersion simulations during the bora wind episode

In order to analyze the characteristics of atmospheric dispersion of pollutants during bora and sirocco wind events, concentrations of black carbon were calculated with FLEXPART-WRF for every half-hour step.

Figure 8 represents the total column mass of tracer per unit area at different times. Tracers carried by bora traveled toward a distinct west-south-westerly direction as expected from the strong bora wind. Initially, before full intensity of bora formed (Figure 8. a), the tracer was carried slowly along the coast. 24 hours after the start of the simulation, bora gained its full strength which is evident in the distribution of the tracer concentrations. As bora is a gusty wind the plume at times loses its primary direction in between gusts. Figure 8.a compared to Figure 8Figure 8.b-f shows a higher concentration accumulated over the islands since only a weak wind was dispersing it, as opposed to the latter times where the residence time of tracer over a grid cell is short due to the higher wind velocities.

The rough time of bora event beginning can be inferred from Figure 7 as the point in time where the concentration starts suddenly increasing with height. Tracer then travels over open sea carried by the wind and gains height as it travels. After the initial, pre-bora, accumulation of tracer at lower altitudes, the concentration is low and well mixed over altitudes ranging from 0-2500 meters.

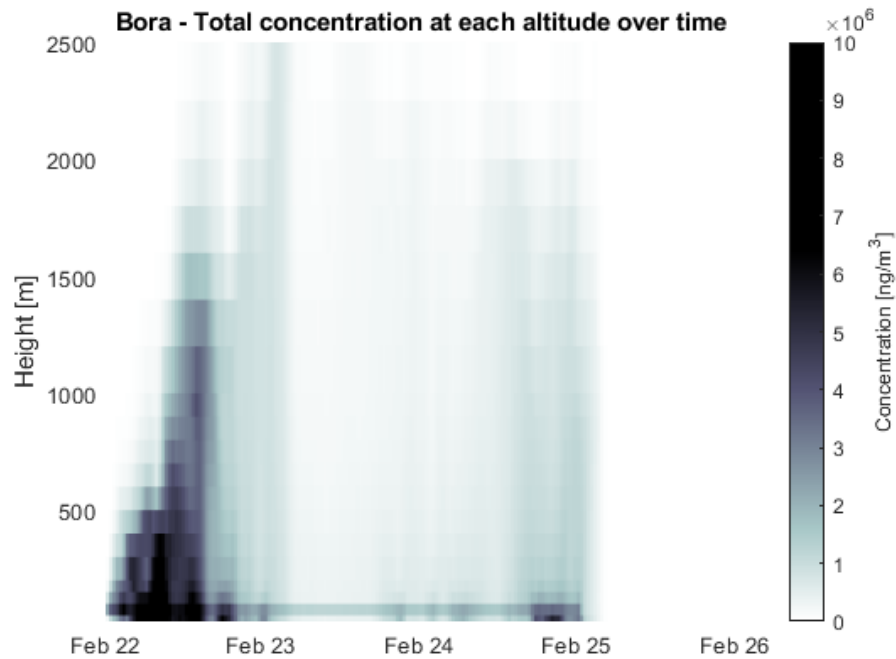


Figure 7. Total concentration at each height level for each time step of the bora simulation. This graph shows the evolution of height of the plume. Data points were obtained by summing concentrations over all latitudes and longitudes for each height level and time step.

The maximum concentrations occurred in the urban Split area downwind of the releases, peaks at $225.6 \mu\text{g}/\text{m}^3$ at the altitude of 25 m before the bora events starts, but its levels quickly drop below $20 \mu\text{g}/\text{m}^3$ where they stay for the duration of the event. The former value is dangerous for sensitive individuals during prolonged exposure, but the latter values were below the dangerous levels set by the World Health Organization (WHO). Pollution carried over the sea crosses the island of Šolta with concentrations lower than $2 \mu\text{g}/\text{m}^3$, posing no danger to human health. By the time the plume reaches Šolta it is well mixed in the boundary layer, as indicated in Figure 9. The island of Brač and Čiovo also experienced a short-term pollution impact when the initial accumulation of pollutant was blown away from Split by bora.

Longer residence time before bora events pollutes the air above the islands and next to the coast, although concentration values never exceed dangerous levels. This may be further examined in a future study to determine if the significant portion of the pollution over the islands is caused by the industrial emissions from Split. This may be done by backwards modelling with concentrations measured on the islands.

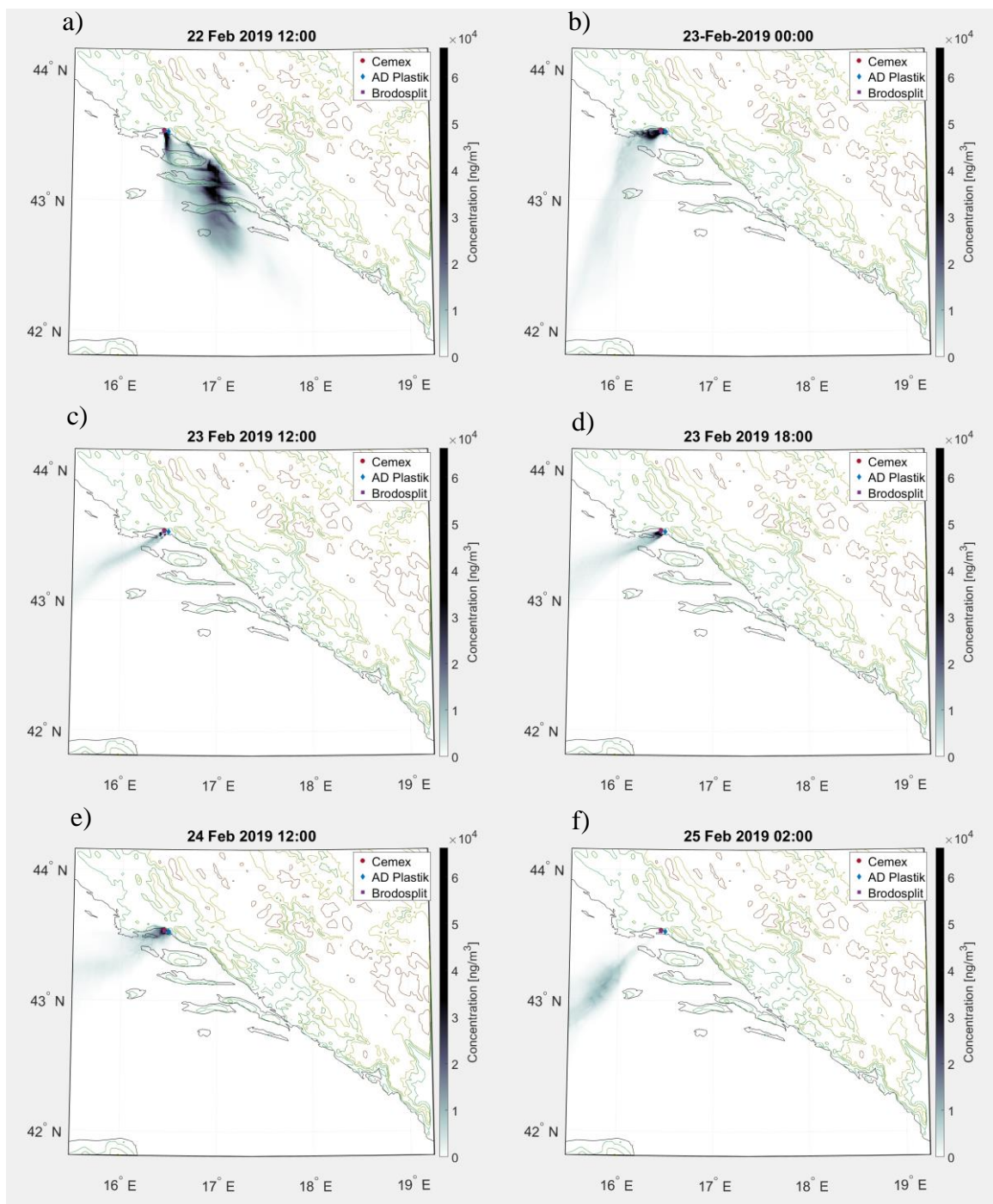


Figure 8.a-f Spatial distributions of column concentration of black carbon for different time steps during the bora simulation. Figure 8.a shows the distribution 12 hours into the simulation but before the bora event properly started. Figures 8.b-f show the distribution during the bora event and corresponds to typical bora behaviour being a fast, strong wind toward south-westerly direction. Contour lines were drawn at 0, 200, 500, 750 and 1500 m.

Tracer leaves the atmosphere due to dry and wet deposition and, in case of bora, only small mass of black carbon is deposited: roughly 10^{-3}g/m^2 by dry deposition and $3 \times 10^{-5} \text{g/m}^2$ by wet deposition out of $3 \times 10^4 \text{kg}$, which is the total emitted mass across all three emitters. Distribution of total dry and wet depositions can be seen in Figure 10 and Figure 11, respectively.

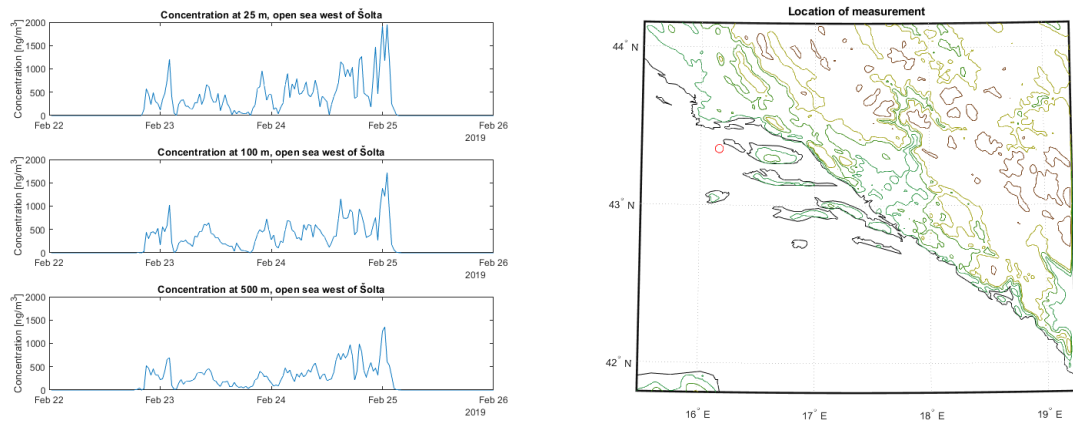


Figure 9. Concentrations of pollutant west of Šolta at 25 m, 100 m and 500 m. Values were below $2 \mu\text{g/m}^3$ and well mixed over the boundary layer.

Dry deposition is localized mostly on the Split peninsula and the surrounding land and if one compared Figure 7 and Figure 12, most of the mass was deposited early in the bora event while the average cloud height was low and the tracer was touching the ground. During the latter part of the bora event almost no mass was dry deposited, and this is due to the atmosphere being well mixed by bora's turbulent gusts.

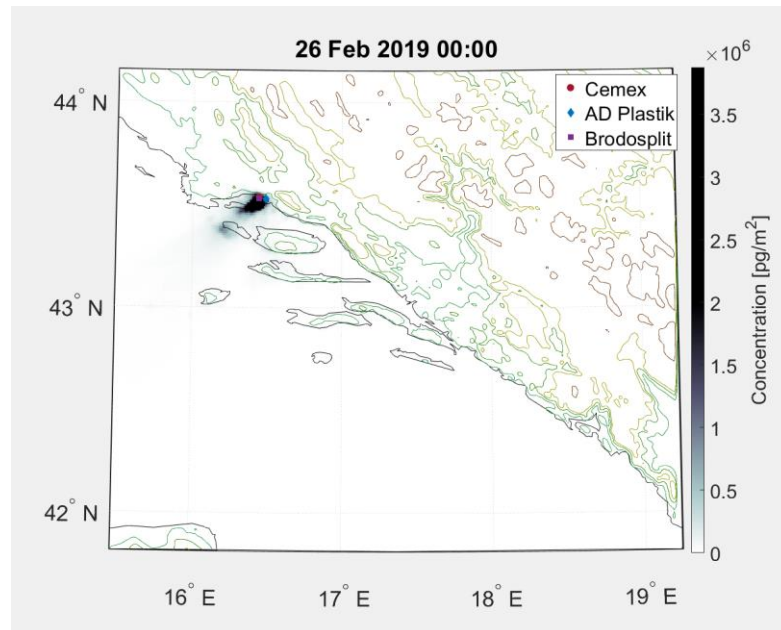


Figure 10. Dry deposition during bora. Deposition is limited in space to areas close to Split peninsula. Wet deposition happens at two distinct moments (Figure 12) and at very low values, two orders of magnitude lower than that of dry deposition. Bora is a dry, continental wind, so this was the expected result. Looking at Figure 11, one can see that the wet deposition during bora occurred over land where one would expect precipitation due to convection.

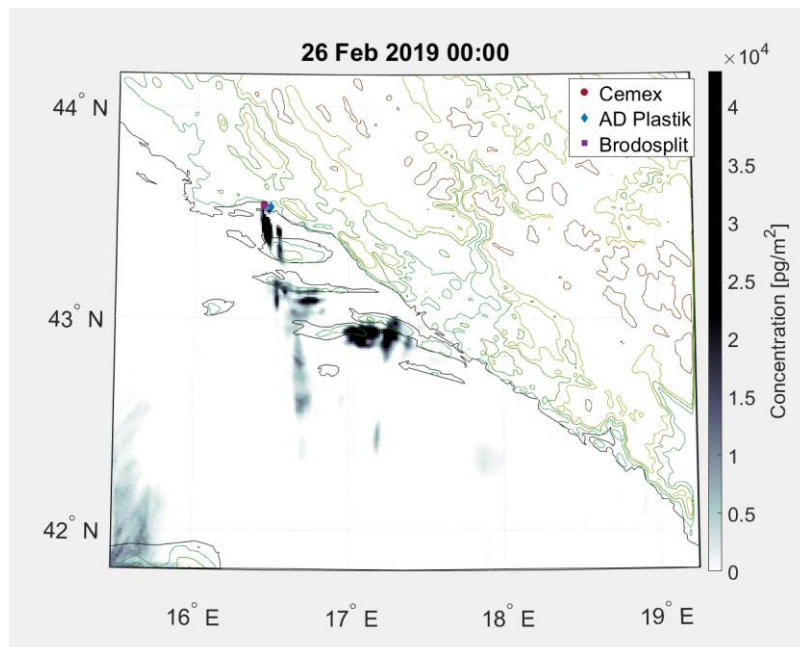


Figure 11. Wet deposition during bora. Notice that the scale is two orders of magnitude smaller than that of dry deposition.

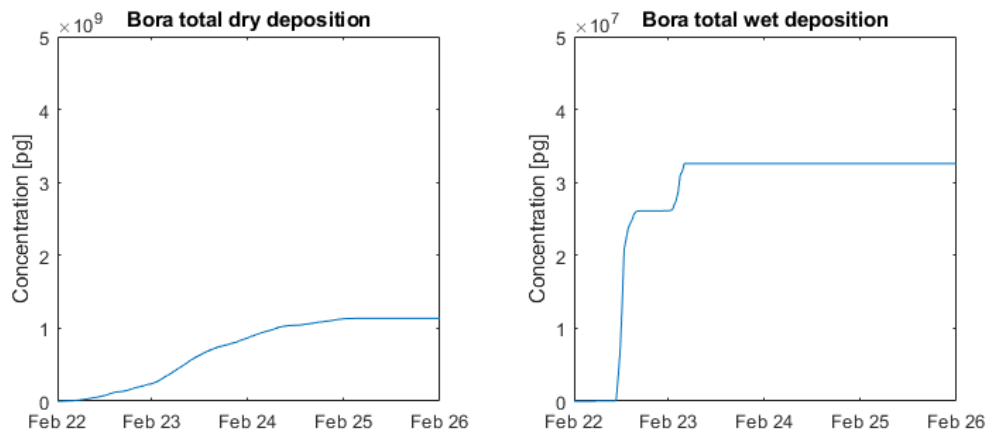


Figure 12. Time series of the total dry and wet depositions during bora. Rate of dry deposition is highest before the plume starts gaining altitude. Wet deposition happens at two distinct moments and at a significantly smaller order of magnitude.

5.2. Dispersion simulations during the sirocco wind episode

During the simulation for sirocco case, the wind starts immediately blowing and thus there is no initial aggregation of concentrations over Split. Dispersion is oriented toward north-west, with the tracer travelling over the coast seemingly not impeded by local terrain. The wind starts weakening during the middle of the third day, sirocco loses its distinct south-south-easterly direction and turns southerly for 12 hours before it becomes completely random.

Figure 15.e shows sirocco losing its south-easterly direction, while in Figure 15.f wind turns to south before again turning north again. Looking at Figure 13. one can see that unlike in the bora case there is no build up of concentrations around the emitters since the wind was already blowing when emissions started.

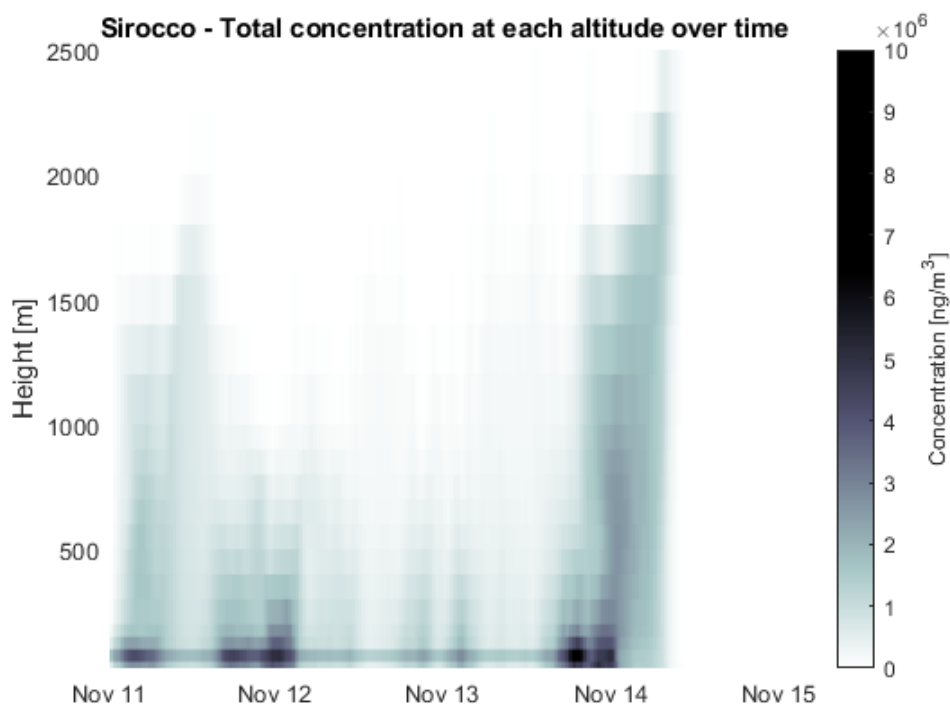


Figure 13. Total concentration at each height level for each time step during the sirocco simulation. This graph shows the evolution of height of the plume. Data points were obtained by summing concentrations over all latitudes and longitudes for each height level and time step.

Concentration then does not increase significantly (i.e., stays on the same order of magnitude) at the lowest altitudes. Sudden increase around November 14 is probably due to the winds turning southward and no concentration leaving the domain. Maximum

concentrations occurred near the release points and downwind toward Kaštela or Čiovo, depending on where the wind was blowing at that time. Peak concentrations occurred in Kaštela ($26.5 \mu\text{g}/\text{m}^3$) and Slatine, Čiovo ($36.6 \mu\text{g}/\text{m}^3$) during the event, and at Split riva ($278.5 \mu\text{g}/\text{m}^3$) for a short time after the sirocco has ended. The plume extends in vertical to roughly 400 meters at these locations with vertical mixing being weaker than in bora case. These concentrations pose no danger to human health by themselves, but in combination with other pollution sources could go over the safety threshold.

Total concentration in the domain was lower during the sirocco event (Figure 14) indicating that for the simulated event sirocco had the higher average speed than bora. The accumulation during the latter hours of the simulation is because wind was dispersing the pollutants out of the domain.

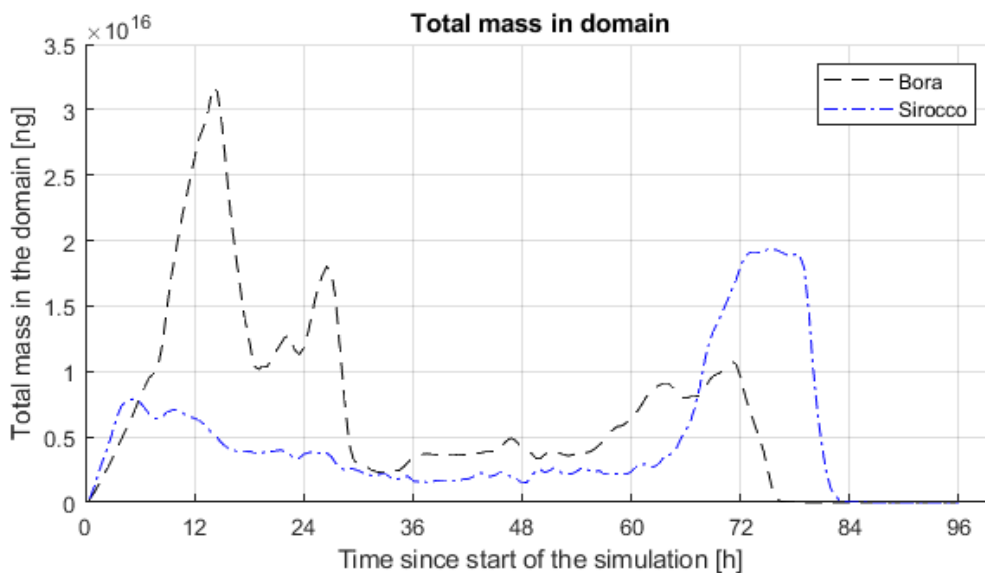


Figure 14. Total mass of pollutant in the domain during the sirocco and bora events. Higher pollutant mass during bora indicates that sirocco had higher average speed than bora since the rate of release was same during both simulations. Accumulation during the latter period of sirocco simulation is due to sirocco weakening and the wind changing direction.

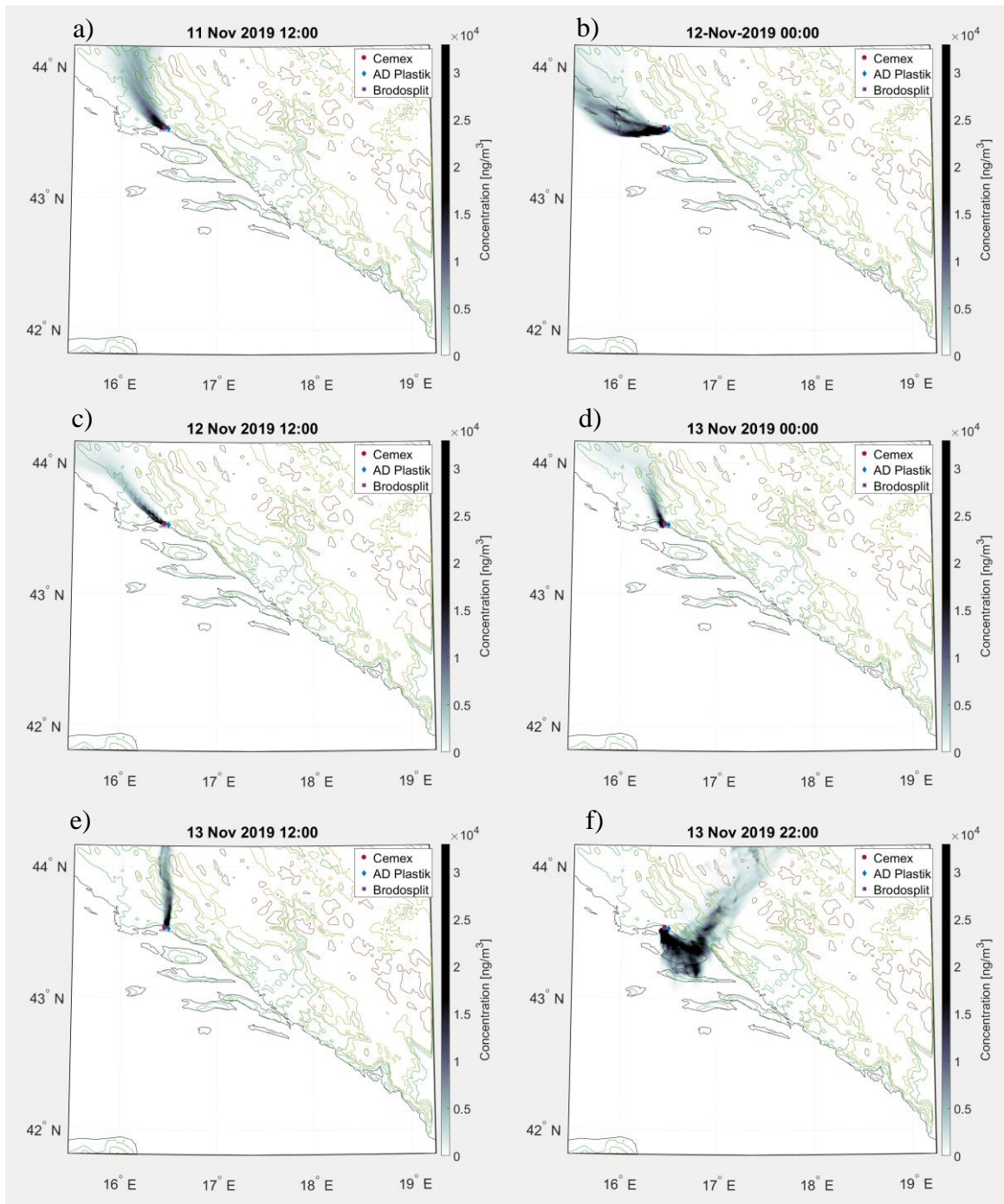


Figure 15.a-f Spatial distributions of column concentration of black carbon for different times during bora simulation. Contour lines were drawn at 0, 200, 500, 750 and 1500 m.

Dry deposition is almost the same as in the bora case, totally depositing roughly 10^{-3} g of black carbon, most on the land closest to the emissions and decreasing with distance. Wet deposition on the other hand is far more pronounced, reaching 3×10^{-3} g of deposited material. Most of the deposition is again closest to the source and decreasing with distance but covers larger area. Stronger wet deposition is to be expected during sirocco since it is a warmer wind coming from the sea and carrying moisture. It can be noted that wet deposition occurred near the coast. This is due to the wind direction carrying the pollutant over that area, but a possible explanation is that it was blocked by terrain.

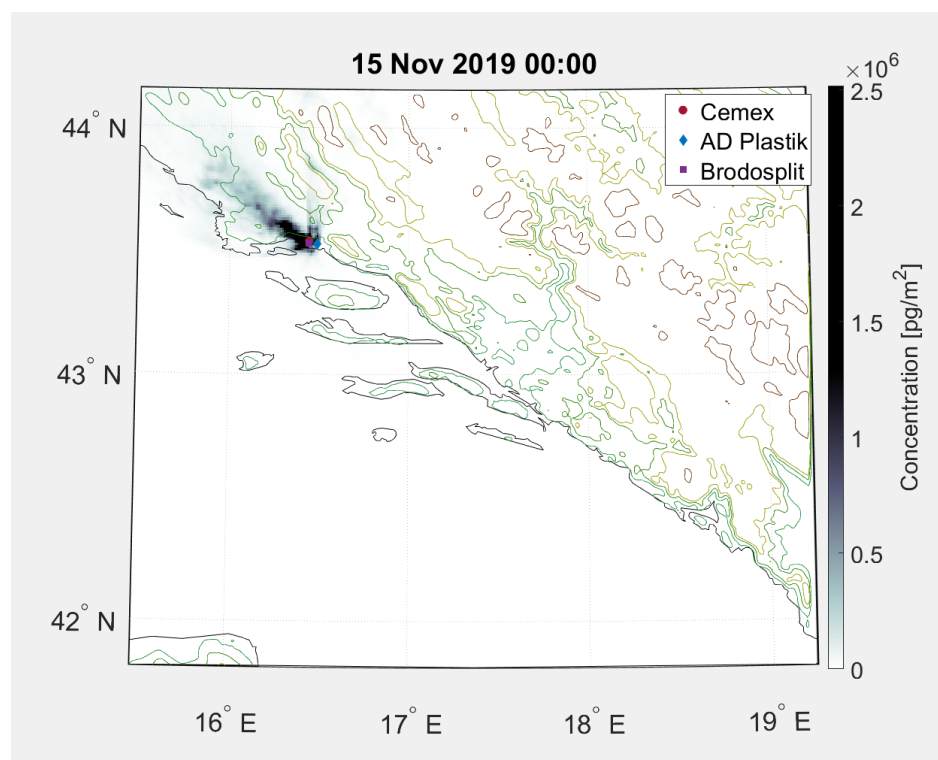


Figure 16. Dry deposition during sirocco. Deposition is located downstream of the wind with highest concentrations nearest to the emission source and decreasing with distance from it.

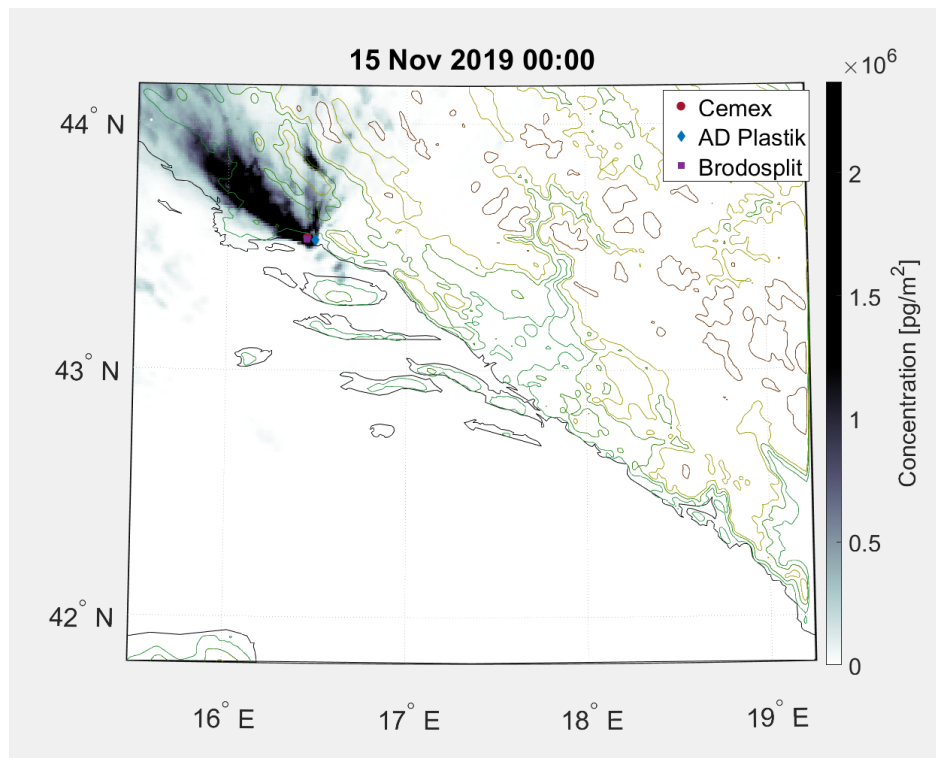


Figure 17. Wet deposition during sirocco. It covers a larger area than dry deposition. Most of the deposition is near the source and decreases with distance from it. Most of the pollutant is wet deposited along the coast and low-lying areas with only small amounts reaching higher altitudes.

Figure 18. shows that the rate of dry deposition is roughly constant during the event before sirocco starts weakening. Wet deposition happens in two distinct episodes: the first is in the early hours of November 12 and ends before noon, while the second begins at the end of the 12th and lasts until the noon of the November 13.

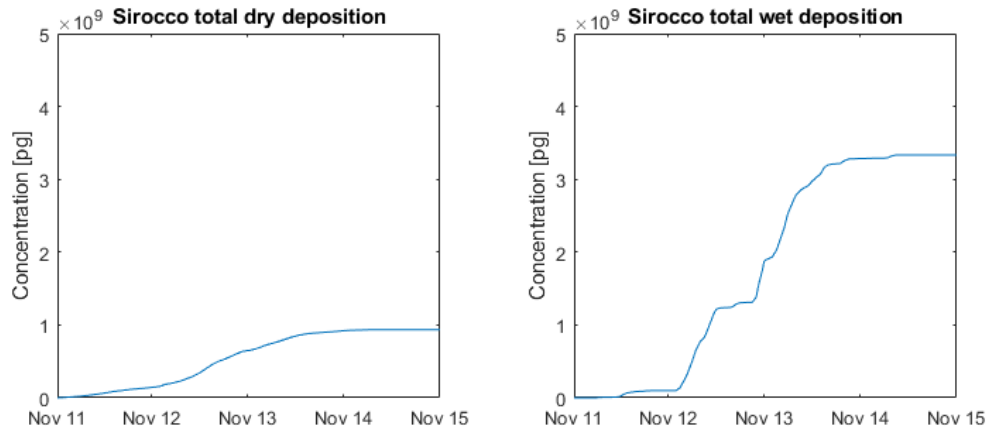


Figure 18. Time series of total dry and wet depositions during sirocco. Dry deposition is roughly constant before sirocco weakens. Wet deposition happens at two distinct episodes, first after midnight, second between midnight and noon.

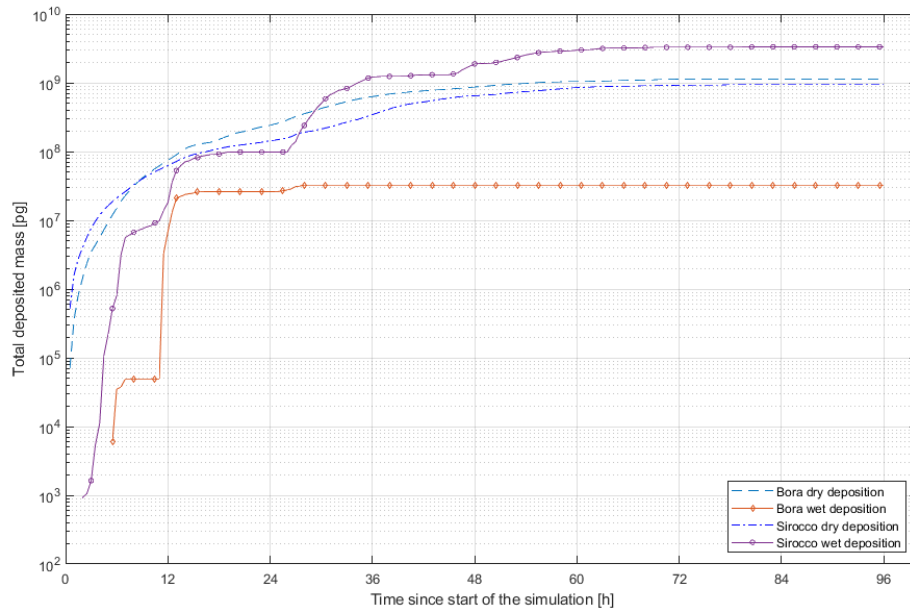


Figure 19. Comparison of time series of total dry and wet deposition during both sirocco and bora. Most pollutant is wet deposited during sirocco, while the least is wet deposited by bora.

6. Conclusion

Dispersion processes during bora and sirocco events over the eastern Adriatic were studied using FLEXPART-WRF dispersion model in order to determine the characteristics and behaviour of the plume evolution. The total mass emitted during both simulations was 10000 kg per source, emitted simultaneously from 3 different locations near Split.

Bora is a dry, gusty, and cold continental north-easterly wind. The city of Split was most affected by the pollution since the main emission sources were located nearby. Pollutants carried by bora were well mixed in the lower atmosphere, up to 6 km, which resulted in low concentrations in the first 12 hours of the event, with an order of magnitude of 1 μg , at sea level and populated areas downwind. Total deposition of the pollutant during the studied period was around 10^{-2} g.

Sirocco is a warm and moist south-easterly wind. Pollutants were carried across Kaštela Bay towards north-west along the coast. It was less well-mixed than during bora, only up to 2 km in height. The most affected areas during the sirocco event were Split, Čiovo, and Kaštela with sea level concentrations being on the order of magnitude of 1 μg .

As expected, the areas closest to the release points and downwind experienced the highest concentrations of pollutants. For both simulations, areas most affected with pollutants were Split, Kaštela, Kaštela Bay and Čiovo island while Šolta and Brač were much less affected. Concentrations higher than 2 μg were simulated in Kaštela, Split, Šolta, Trogir, and even 60 kilometres north-west of the release points.

Most mass was wet deposited by sirocco and the least was dry deposited by bora. The deposited mass is less than 10^{-2} g in all cases.

Further research could include a larger number of bora and sirocco events, both extreme and non-extreme cases. Backward mode could be utilized to determine the sources of pollution if one obtains the measured concentrations. Real emission data could also be compared with the results to validate the simulations. Larger domain could be used to determine the actual reach of the plume.

7. Literature

- [1] Orlic et al. (1994). Response of the Adriatic Sea to the bora and scirocco forcing. 14 (1), 91-116, [https://doi.org/10.1016/0278-4343\(94\)90007-8](https://doi.org/10.1016/0278-4343(94)90007-8)
- [2] Objektivna ocjena kvalitete zraka u zonama Republike Hrvatske za 2017. godinu. <http://iszz.azo.hr/iskzl/datoteka?id=80839> (last access: 12.9.2021.)
- [3] Smith, R. B. (1987). Aerial Observations of the Yugoslavian Bora, Journal of Atmospheric Sciences, 44(2), 269-297, [https://doi.org/10.1175/1520-0469\(1987\)044<0269:AOOTYB>2.0.CO;2](https://doi.org/10.1175/1520-0469(1987)044<0269:AOOTYB>2.0.CO;2)
- [4] Grisogono, B. and Belušić, D. (2009), A review of recent advances in understanding the meso- and microscale properties of the severe Bora wind. Tellus A, 61, 1-16. <https://doi.org/10.1111/j.1600-0870.2008.00369.x>
- [5] Ulbrich, Uwe & Lionello, P. & Belusic, Danijel & Jacobeit, Jucundus & Knippertz, Peter & Kuglitsch, Franz Gunther & Leckebusch, G.C. & Luterbacher, Jürg & Maugeri, Maurizio & Maheras, Panagiotis & Nissen, Katrin & Pavan, Valentina & Pinto, Joaquim & Saaroni, Hadas & Seubert, S. & Toreti, Andrea & Xoplaki, Elena & Ziv, Baruch. (2012). Climate of the Mediterranean: Synoptic Patterns, Temperature, Precipitation, Winds, and Their Extremes, 301 – 346, Elsevier
- [6] Defant, F. (1951). Compendium of Meteorology. 669–670.
- [7] Pasarić, Z., Belušić, D., and Klaić, Z. B. (2007). Orographic influences on the Adriatic sirocco wind, Ann. Geophys., 25, 1263–1267, <https://doi.org/10.5194/angeo-25-1263-2007>,.
- [8] Orlic, Mirko & Kuzmić, Milivoj & Pasarić, Z.. (1994). Response of the Adriatic Sea to the Bora and sirocco forcing. Continental Shelf Research. 14. 91-116. [https://doi.org/10.1016/0278-4343\(94\)90007-8](https://doi.org/10.1016/0278-4343(94)90007-8)
- [9] Ivančan-Picek B, Jurčec V, Drvar D. On the causes of Adriatic jugo wind variations. Hrvatski meteorološki časopis 41, br. 41. 2006 [last accessed 13.08.2021]. <https://hrcak.srce.hr/64347>
- [10] Ivančan-Picek, Branka & Jurcec, Vesna & Tutis, Vlasta & Vukicevic, Vlatko. (1996). Severe Adriatic jugo wind. Meteorologische Zeitschrift. 5. 67-75.
- [11] Cushman-Roisin, Beckers (2011). Introduction to Geophysical Fluid Dynamics: Physical and Numerical Aspects, 2nd Edition., Elsevier

- [12] Robert H. Stewart (2000.), Introduction To Physical Oceanography, Department of Oceanography, Texas A & M University
- [13] Koracin, D. et al. (2011.) “Regional Source Identification Using Lagrangian Stochastic Particle Dispersion and HYSPLIT Backward-Trajectory Models.” *Journal of the Air & Waste Management Association* 61 (2011): 660 – 672.
<https://doi.org/10.3155/1047-3289.61.6.660>
- [14] Stohl, A., Forster, C., Frank, A., Seibert, P., and Wotawa, G. (2005). Technical note: The Lagrangian particle dispersion model FLEXPART version 6.2, *Atmos. Chem. Phys.*, 5, 2461–2474, <https://doi.org/10.5194/acp-5-2461-2005>
- [15] Brioude, J., Arnold, D., Stohl, A., Cassiani, M., Morton, D., Seibert, P., Angevine, W., Evan, S., Dingwell, A., Fast, J. D., Easter, R. C., Pisso, I., Burkhardt, J., and Wotawa, G. (2013). The Lagrangian particle dispersion model FLEXPART-WRF version 3.1, *Geosci. Model Dev.*, 6, 1889–1904, <https://doi.org/10.5194/gmd-6-1889-2013>
- [16] Madala, Srikanth & Prasad, K. & C., Venkata Srinivas & Satyanarayana, A.N.V.. (2016). Air quality simulation of NOX over the tropical coastal city Chennai in southern India with FLEXPART-WRF. *Atmospheric Environment*. 128. 65-81.
<https://doi.org/10.1016/j.atmosenv.2015.12.052>
- [17] Kivimaki, E. J., (2016). Source areas and effect of wet deposition on particles detected at SMEAR II measurement station as studied with FLEXPART [Master's thesis, University of Helsinki]
https://helda.helsinki.fi/bitstream/handle/10138/169525/kivimaki_mastersthesis.pdf
- [18] Hanna S.R. (1984) Applications in Air Pollution Modeling. In: Nieuwstadt F.T.M., van Dop H. (eds) *Atmospheric Turbulence and Air Pollution Modelling*. Atmospheric Sciences Library, vol 1. Springer, Dordrecht.
https://doi.org/10.1007/978-94-010-9112-1_7
- [19] Ambient (outdoor) air pollution (22 September 2021) [last accessed 14.01.2022.]
[https://www.who.int/news-room/fact-sheets/detail/ambient-\(outdoor\)-air-quality-and-health](https://www.who.int/news-room/fact-sheets/detail/ambient-(outdoor)-air-quality-and-health)

8. Appendix

8.1. Bora input file:

```
=====FORMER PATHNAMES FILE=====
/mnt/beegfs/user/denk/bora/output/
/mnt/beegfs/user/denk/Wrfddata/
/mnt/beegfs/user/denk/bora/AVAILABLE_b
=====
=====FORMER COMMAND FILE=====
 1          LDIRECT:          1 for forward simulation, -1 for backward simulation
20190222 000000 YYYMMDD HHMISS beginning date of simulation
20190226 000000 YYYMMDD HHMISS ending date of simulation
1800       SSSSS (int)       output every SSSSS seconds
1800       SSSSS (int)       time average of output (in SSSSS seconds)
180        SSSSS (int)       sampling rate of output (in SSSSS seconds)
999999999  SSSSS (int)       time constant for particle splitting (in seconds)
180        SSSSS (int)       synchronisation interval of flexpart (in seconds)
10.        CTL (real)       factor by which time step must be smaller than t1
10         IFINE (int)      decrease of time step for vertical motion by factor ifine
5          IOUT              1 concentration, 2 mixing ratio, 3 both, 4 plume traject, 5=1+4
0          IPOUT            particle dump: 0 no, 1 every output interval, 2 only at end
1          LSUBGRID        subgrid terrain effect parameterization: 1 yes, 0 no
0          LCONVECTION     convection: 3 yes, 0 no
3600.     DT_CONV (real)   time interval to call convection, seconds
0         LAGESPECTRA     age spectra: 1 yes, 0 no
0         IPIN             continue simulation with dumped particle data: 1 yes, 0 no
0         IFLUX            calculate fluxes: 1 yes, 0 no
0         IOUTPUTFOREACHREL CREATE AN OUPUT FILE FOR EACH RELEASE LOCATION: 1 YES, 0 NO
0         MDOMAINFILL     domain-filling trajectory option: 1 yes, 0 no, 2 strat. o3 tracer
1         IND_SOURCE       1=mass unit , 2=mass mixing ratio unit
1         IND_RECEPTOR   1=mass unit , 2=mass mixing ratio unit
0         NESTED_OUTPUT    shall nested output be used? 1 yes, 0 no
```


0	LINIT_COND	INITIAL COND. FOR BW RUNS: 0=NO,1=MASS UNIT,2=MASS MIXING RATIO UNIT
1	TURB_OPTION	0=no turbulence; 1=diagnosed as in flexpart_ecmwf; 2 and 3=from tke.
1	LU_OPTION	0=old landuse (IGBP.dat); 1=landuse from WRF
1	CBL_SCHEME	0=no, 1=yes. works if TURB_OPTION=1
0	SFC_OPTION	0=default computation of u*, hflux, pblh, 1=from wrf
0	WIND_OPTION	0=snapshot winds, 1=mean winds,2=snapshot eta-dot,-1=w based on divergence
0	TIME_OPTION	1=correction of time validity for time-average wind, 0=no need
1	OUTGRID_COORD	0=wrf grid(meters), 1=regular lat/lon grid
1	RELEASE_COORD	0=wrf grid(meters), 1=regular lat/lon grid
2	IOUTTYPE	0=default binary, 1=ascii (for particle dump only),2=netcdf
999	NCTIMEREC (int)	Time frames per output file, only used for netcdf
100	VERBOSE	VERBOSE MODE,0=minimum, 100=maximum
=====FORMER AGECLASESS FILE=====		
1	NAGECLASS	number of age classes
9999	SSSSSS (int)	age class in SSSSS seconds
=====FORMER OUTGRID FILE=====		
15.483246	OUTLONLEFT	geographical longitude of lower left corner of output grid
41.808704	OUTLATLOWER	geographical latitude of lower left corner of output grid
350	NUMXGRID	number of grid points in x direction (= # of cells)
230	NUMYGRID	number of grid points in y direction (= # of cells)
1	OUTGRIDDEF	outgrid defined 0=using grid distance, 1=upperright corner coordinate
19.244263	DXOUTLON	grid distance in x direction or upper right corner of output grid
44.157829	DYOUTLON	grid distance in y direction or upper right corner of output grid
25	NUMZGRID	number of vertical levels
25.0	LEVEL	height of level (upper boundary)
50.0	LEVEL	height of level (upper boundary)
100.0	LEVEL	height of level (upper boundary)
150.0	LEVEL	height of level (upper boundary)
200.0	LEVEL	height of level (upper boundary)
300.0	LEVEL	height of level (upper boundary)
400.0	LEVEL	height of level (upper boundary)
500.0	LEVEL	height of level (upper boundary)
600.0	LEVEL	height of level (upper boundary)
700.0	LEVEL	height of level (upper boundary)
800.0	LEVEL	height of level (upper boundary)
900.0	LEVEL	height of level (upper boundary)
1000.0	LEVEL	height of level (upper boundary)
1200.0	LEVEL	height of level (upper boundary)

```

1400.0      LEVEL      height of level (upper boundary)
1600.0      LEVEL      height of level (upper boundary)
1800.0      LEVEL      height of level (upper boundary)
2000.0      LEVEL      height of level (upper boundary)
2250.0      LEVEL      height of level (upper boundary)
2500.0      LEVEL      height of level (upper boundary)
2750.0      LEVEL      height of level (upper boundary)
3000.0      LEVEL      height of level (upper boundary)
4000.0      LEVEL      height of level (upper boundary)
6000.0      LEVEL      height of level (upper boundary)
20000.0     LEVEL      height of level (upper boundary)
=====FORMER RECEPTOR FILE=====
0           NUMRECEPTOR  number of receptors
=====FORMER SPECIES FILE=====
1           NUMTABLE      number of variable properties. The following lines are fixed format
XXXX|NAME      |decaytime |wetscava  |wetsb|drydif|dryhenry|drya|partrho  |parmean|partsig|dryvelo|weight |
BC          -999.9  1.0E-04  0.80  -9.9          2.0E03 4.0E-07  0.3  -9.99  100.00
=====FORMER RELEASES FILE=====
1           NSPEC         total number of species emitted
0           EMITVAR       1 for emission variation
1           LINK          index of species in file SPECIES
3           NUMPOINT      number of releases
20190222 000000 ID1, IT1      beginning date and time of release
20190225 000000 ID2, IT2      ending date and time of release
16.440905 XPOINT1 (real) longitude [deg] of lower left corner
43.540889 YPOINT1 (real) latitude [deg] of lower left corner
16.440905 XPOINT2 (real) longitude [deg] of upper right corner
43.540889 YPOINT2 (real) latitude [DEG] of upper right corner
2           KINDZ (int) 1 for m above ground, 2 for m above sea level, 3 pressure
50.000    ZPOINT1 (real) lower z-level
50.000    ZPOINT2 (real) upper z-level
1000000   NPART (int) total number of particles to be released
1.000E+04 XMASS (real) total mass emitted
cemex     NAME OF RELEASE LOCATION
20190222 000000 ID1, IT1      beginning date and time of release
20190225 000000 ID2, IT2      ending date and time of release
16.486364 XPOINT1 (real) longitude [deg] of lower left corner
43.529463 YPOINT1 (real) latitude [deg] of lower left corner

```

```

16.486364      XPOINT2 (real)  longitude [deg] of upper right corner
43.529463      YPOINT2 (real)  latitude [DEG] of upper right corner
      2        KINDZ  (int)  1 for m above ground, 2 for m above sea level, 3 pressure
50.000        ZPOINT1 (real)  lower z-level
50.000        ZPOINT2 (real)  upper z-level
1000000       NPART  (int)    total number of particles to be released
1.000E+04     XMASS  (real)    total mass emitted
adplastik     NAME OF RELEASE LOCATION
20190222 000000 ID1, IT1      beginning date and time of release
20190225 000000 ID2, IT2      ending date and time of release
16.440589     XPOINT1 (real)  longitude [deg] of lower left corner
43.525121     YPOINT1 (real)  latitude [deg] of lower left corner
16.440589     XPOINT2 (real)  longitude [deg] of upper right corner
43.525121     YPOINT2 (real)  latitude [DEG] of upper right corner
      2        KINDZ  (int)  1 for m above ground, 2 for m above sea level, 3 pressure
50.000        ZPOINT1 (real)  lower z-level
50.000        ZPOINT2 (real)  upper z-level
1000000       NPART  (int)    total number of particles to be released
1.000E+04     XMASS  (real)    total mass emitted
brodosplit    NAME OF RELEASE LOCATION

```

8.2. Sirocco input file

```

=====FORMER PATHNAMES FILE=====
/mnt/beegfs/user/denk/sirocco/output/
/mnt/beegfs/user/denk/Wrfdata/
/mnt/beegfs/user/denk/sirocco/AVAILABLE_s
=====
=====FORMER COMMAND FILE=====
 1          LDIRECT:          1 for forward simulation, -1 for backward simulation
20191111 000000 YYYMMDD HHMISS beginning date of simulation
20191115 000000 YYYMMDD HHMISS ending date of simulation
1800       SSSSS (int)       output every SSSSS seconds
1800       SSSSS (int)       time average of output (in SSSSS seconds)
180        SSSSS (int)       sampling rate of output (in SSSSS seconds)
999999999  SSSSS (int)       time constant for particle splitting (in seconds)
180        SSSSS (int)       synchronisation interval of flexpart (in seconds)
10.        CTL (real)       factor by which time step must be smaller than t1
10         IFINE (int)      decrease of time step for vertical motion by factor ifine
5          IOUT              1 concentration, 2 mixing ratio, 3 both, 4 plume traject, 5=1+4
0          IPOUT            particle dump: 0 no, 1 every output interval, 2 only at end
1          LSUBGRID        subgrid terrain effect parameterization: 1 yes, 0 no
0          LCONVECTION     convection: 3 yes, 0 no
3600.     DT_CONV (real)   time interval to call convection, seconds
0         LAGESPECTRA     age spectra: 1 yes, 0 no
0         IPIN             continue simulation with dumped particle data: 1 yes, 0 no
0         IFLUX           calculate fluxes: 1 yes, 0 no
0         IOUTPUTFOREACHREL CREATE AN OUPUT FILE FOR EACH RELEASE LOCATION: 1 YES, 0 NO
0         MDOMAINFILL     domain-filling trajectory option: 1 yes, 0 no, 2 strat. o3 tracer
1         IND_SOURCE      1=mass unit , 2=mass mixing ratio unit
1         IND_RECEPTOR  1=mass unit , 2=mass mixing ratio unit
0         NESTED_OUTPUT   shall nested output be used? 1 yes, 0 no
0         LINIT_COND     INITIAL COND. FOR BW RUNS: 0=NO,1=MASS UNIT,2=MASS MIXING RATIO UNIT
1         TURB_OPTION    0=no turbulence; 1=diagnosed as in flexpart_ecmwf; 2 and 3=from tke.
1         LU_OPTION      0=old landuse (IGBP.dat); 1=landuse from WRF
1         CBL_SCHEME     0=no, 1=yes. works if TURB_OPTION=1
0         SFC_OPTION     0=default computation of u*, hflux, pblh, 1=from wrf
0         WIND_OPTION    0=snapshot winds, 1=mean winds,2=snapshot eta-dot,-1=w based on divergence

```

```

0          TIME_OPTION      1=correction of time validity for time-average wind, 0=no need
1          OUTGRID_COORD    0=wrf grid(meters), 1=regular lat/lon grid
1          RELEASE_COORD    0=wrf grid(meters), 1=regular lat/lon grid
2          IOUTTYPE         0=default binary, 1=ascii (for particle dump only),2=netcdf
999       NCTIMEREC (int)    Time frames per output file, only used for netcdf
100      VERBOSE           VERBOSE MODE,0=minimum, 100=maximum
=====FORMER AGECLASSESS FILE=====
1          NAGECLASS        number of age classes
9999     SSSSSS (int)       age class in SSSSSS seconds
=====FORMER OUTGRID FILE=====
15.483246 OUTLONLEFT       geographical longitude of lower left corner of output grid
41.808704 OUTLATLOWER      geographical latitude of lower left corner of output grid
350      NUMXGRID          number of grid points in x direction (= # of cells )
230      NUMYGRID          number of grid points in y direction (= # of cells )
1        OUTGRIDDEF       outgrid defined 0=using grid distance, 1=upperright corner coordinate
19.244263 DXOUTLON        grid distance in x direction or upper right corner of output grid
44.157829   DYOUTLON      grid distance in y direction or upper right corner of output grid
25        NUMZGRID        number of vertical levels
25.0      LEVEL           height of level (upper boundary)
50.0      LEVEL           height of level (upper boundary)
100.0     LEVEL           height of level (upper boundary)
150.0     LEVEL           height of level (upper boundary)
200.0     LEVEL           height of level (upper boundary)
300.0     LEVEL           height of level (upper boundary)
400.0     LEVEL           height of level (upper boundary)
500.0     LEVEL           height of level (upper boundary)
600.0     LEVEL           height of level (upper boundary)
700.0     LEVEL           height of level (upper boundary)
800.0     LEVEL           height of level (upper boundary)
900.0     LEVEL           height of level (upper boundary)
1000.0    LEVEL           height of level (upper boundary)
1200.0    LEVEL           height of level (upper boundary)
1400.0    LEVEL           height of level (upper boundary)
1600.0    LEVEL           height of level (upper boundary)
1800.0    LEVEL           height of level (upper boundary)
2000.0    LEVEL           height of level (upper boundary)
2250.0    LEVEL           height of level (upper boundary)
2500.0    LEVEL           height of level (upper boundary)

```

```

2750.0          LEVEL          height of level (upper boundary)
3000.0          LEVEL          height of level (upper boundary)
4000.0          LEVEL          height of level (upper boundary)
6000.0          LEVEL          height of level (upper boundary)
20000.0         LEVEL          height of level (upper boundary)
=====FORMER RECEPTOR FILE=====
0              NUMRECEPTOR   number of receptors
=====FORMER SPECIES FILE=====
1              NUMTABLE        number of variable properties. The following lines are fixed format
XXXX|NAME      |decaytime |wetscava  |wetsb|drydif|dryhenry|drya|partrho  |parmean|partsig|dryvelo|weight |
BC          -999.9  1.0E-04   0.8  -9.9                2.0E03 4.0E-07    0.3  -9.99  100.00
=====FORMER RELEASERS FILE=====
1              NSPEC           total number of species emitted
0              EMITVAR         1 for emission variation
1              LINK            index of species in file SPECIES
3              NUMPOINT        number of releases
20191111 000000  ID1, IT1      beginning date and time of release
20191114 000000  ID2, IT2      ending date and time of release
16.440905  XPOINT1 (real) longitude [deg] of lower left corner
43.540889  YPOINT1 (real) latitude [deg] of lower left corner
16.440905  XPOINT2 (real) longitude [deg] of upper right corner
43.540889  YPOINT2 (real) latitude [DEG] of upper right corner
2          KINDZ  (int)  1 for m above ground, 2 for m above sea level, 3 pressure
50.000     ZPOINT1 (real)  lower z-level
50.000     ZPOINT2 (real)  upper z-level
1000000    NPART (int)    total number of particles to be released
1.000E+04  XMASS (real)    total mass emitted
cemex      NAME OF RELEASE LOCATION
20191111 000000  ID1, IT1      beginning date and time of release
20191114 000000  ID2, IT2      ending date and time of release
16.486364  XPOINT1 (real) longitude [deg] of lower left corner
43.529463  YPOINT1 (real) latitude [deg] of lower left corner
16.486364  XPOINT2 (real) longitude [deg] of upper right corner
43.529463  YPOINT2 (real) latitude [DEG] of upper right corner
2          KINDZ  (int)  1 for m above ground, 2 for m above sea level, 3 pressure
50.000     ZPOINT1 (real)  lower z-level
50.000     ZPOINT2 (real)  upper z-level
1000000    NPART (int)    total number of particles to be released

```

```

1.000E+04      XMASS (real)      total mass emitted
adplastik      NAME OF RELEASE LOCATION
20191111 000000 ID1, IT1      beginning date and time of release
20191114 000000 ID2, IT2      ending date and time of release
16.440589     XPOINT1 (real) longitude [deg] of lower left corner
43.525121     YPOINT1 (real) latitude [deg] of lower left corner
16.440589     XPOINT2 (real) longitude [deg] of upper right corner
43.525121     YPOINT2 (real) latitude [DEG] of upper right corner
              2      KINDZ (int) 1 for m above ground, 2 for m above sea level, 3 pressure
50.000        ZPOINT1 (real) lower z-level
50.000        ZPOINT2 (real) upper z-level
1000000       NPART (int)      total number of particles to be released
1.000E+04      XMASS (real)      total mass emitted
brodosplit    NAME OF RELEASE LOCATION

```